Volume 2 | Number 9 | September 2015

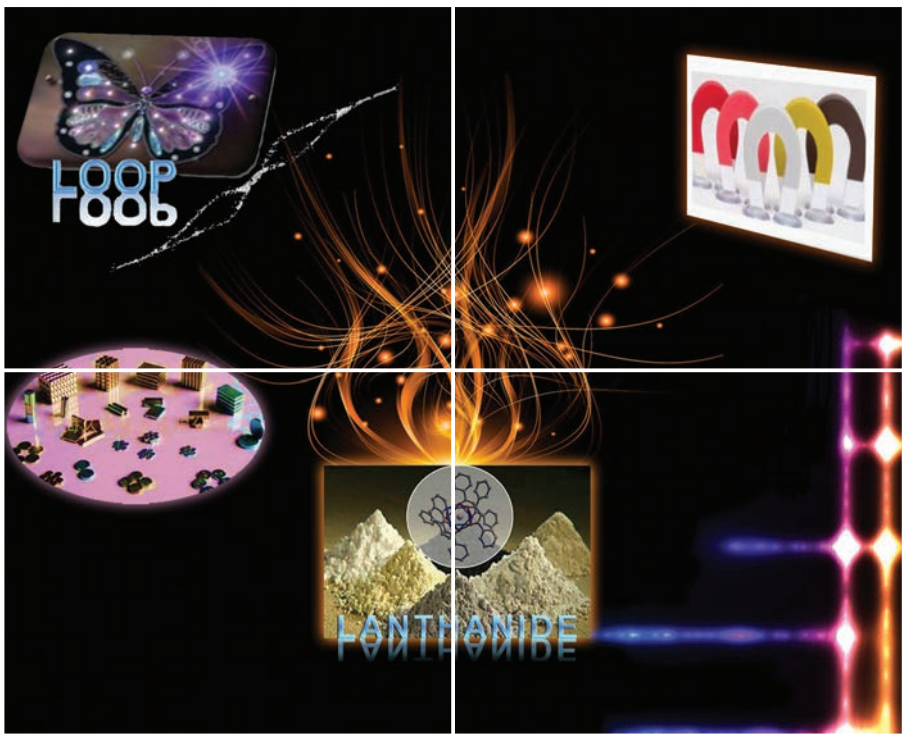

INORGANIC CHEMISTRY

FRONTIERS

Chinese Chemical Society
PEKING UNIVERSITY 1898
ROYAL SOCIETY OF CHEMISTRY

http://rsc.li/frontiers-inorganic

INORGANIC CHEMISTRY
FRONTIERS

RESEARCH ARTICLE

Cite this: *Inorg. Chem. Front.*, 2015, **2**, 837

Transition from isolated to interacting copper(II) pairs in extended lattices evaluated by single crystal EPR spectroscopy†

Nicolás I. Neuman,[a] Emerson Burna,[a] Ricardo Baggio,[b] Mario C. G. Passeggi,[a] Alberto C. Rizzi[a] and Carlos D. Brondino*[a]

We report the synthesis and X-ray structure of the dimeric zinc(II) compound $[Zn(tda)(phen)]_2 \cdot H_2tda$, (tda = thiodiacetic acid, phen = 1,10-phenanthroline) hereafter Zn(tda)(phen), and a single crystal EPR study of Zn(tda)(phen) doped with Cu(II) ions. Zn(tda)(phen) is isomorphous to its Cu(II) analogue. The EPR spectra show a central signal composed of one to four resonances assigned to Cu–Zn heterodimers, flanked by less intense satellite signals assigned to Cu–Cu homodimers. Analysis of single crystal EPR data allowed us to determine the **g**- and **A**-matrices of the Cu(II) ion and the anisotropic ZFS parameters of the homodimer. Within the experimental error, the Cu(II) **g**-matrix obtained for the diluted compound was identical to that previously determined by us in pure Cu(tda)(phen). The ZFS is shown to be dominated by magnetic dipolar coupling between the unpaired electrons mainly centered around the Cu(II) ions, although partially delocalized over the equatorial copper ligands. DFT calculations yielded spin population values compatible with those determined from the analysis of the anisotropic ZFS assuming a distributed dipole model. The information obtained from the diluted compound was used to evaluate the interdimeric exchange interaction between dimeric units in pure Cu(tda)(phen). The comparison between both point and distributed dipole approximations is discussed with reference to the analysis of the EPR data.

Received 29th May 2015,
Accepted 6th July 2015

DOI: 10.1039/c5qi00086f

rsc.li/frontiers-inorganic

Introduction

The study of exchange-coupled transition metal ion complexes has played an important role in the development of the field of molecular magnetism.[1–4] The information gained with these studies has been essential to establish the underlying molecular bases to design not only paramagnetic materials with predictable magnetic properties[5,6] but also to design materials such as molecular-based and single-molecule magnets.[7–11] These studies have also been relevant in biology because exchange-coupled transition metal ion systems occur in proteins in which the superexchange pathways are involved in electron-transfer reactions.[12–16] Thus, the characterization of exchange coupled systems is nowadays a multidisciplinary research field owing to their applications in chemistry, biology, and physics.

Among the vast number of studies on paramagnetic transition metal ion complexes, the study of dinuclear Cu(II) compounds (S = 1/2 spin pair) has been essential in the development of molecular magnetism.[4,17–19] The electronic properties of these metal systems are determined by the isotropic exchange interaction, which couples the two individual electron spins (S = 1/2) to yield singlet (S = 0) and triplet (S = 1) states, and other interactions such as anisotropic and antisymmetric exchange and dipolar magnetic coupling.[20] The isotropic exchange interaction ($H_{ex} = -J\mathbf{S}_1 \cdot \mathbf{S}_2$) splits the singlet from the triplet state of the dimer by an energy amount J, whereas the remaining interactions can remove the three-fold degeneration of the triplet state even in zero magnetic field (ZFS). Additional splitting of the energy levels can be produced by hyperfine interactions with the copper nucleus (I = 3/2). Furthermore, in weakly exchange-coupled dimers the anisotropic interactions can appreciably mix the singlet and triplet states, in which case these states cannot be considered pure. However, the singlet–triplet nomenclature will be used throughout the text for simplicity.

In undiluted magnetic systems, the dimeric units of the crystal lattice may interact with their neighbors through different kinds of chemical paths that may transmit weak

[a]*Departamento de Física, Facultad de Bioquímica y Ciencias Biológicas, Universidad Nacional del Litoral, S3000ZAA Santa Fe, Argentina.*
E-mail: brondino@fbcb.unl.edu.ar
[b]*Gerencia de Investigación y Aplicaciones, Comisión Nacional de Energía Atómica, Avenida Gral Paz y Constituyentes, San Martín, Buenos Aires, Argentina*

†Electronic supplementary information (ESI) available: Single crystal mounting details for the EPR experiment, additional structural data together with structural figures for Zn(tda)(phen), electronic structure calculation results, and figures containing the angular variation of the **A**- and **D**-matrices. CCDC 1055076. For ESI and crystallographic data in CIF or other electronic format see DOI: 10.1039/c5qi00086f

exchange interactions, hereafter designated as J'. This interaction modulates the magnetic behavior of the dimer leading to situations called weak (J' < ZFS), intermediate ($J' \sim$ ZFS), or strong (J' > ZFS) exchange, which can be visualized by single crystal EPR spectroscopy due to the dependence of ZFS with the magnetic field orientation.[20,21] For weak exchange, some features of the dimeric behavior can be detected, as EPR may show, besides the forbidden half field transition corresponding to $\Delta M_S = 2$, two resonance lines of the triplet state, as expected for a dinuclear unit, but shifted to the center of the spectra and broadened; the larger J', the larger the shift and broadening. Particularly, for $J' > A$, where A is the hyperfine constant with the copper nuclei ($I = 3/2$), no hyperfine structure is observed although it can be partially solved for situations with $J' < A$.[22,23] In contrast, for strong exchange, the two triplet lines coming from each dimeric unit merge into one absorption line.

The compound $[Cu(tda)(phen)]_2 \cdot H_2tda$ (tda = thiodiacetate, phen = 1,10-phenanthroline), hereafter Cu(tda)(phen), is a ferromagnetically exchange coupled dimer ($J = +3.2$ cm^{-1}), in which we determined that very weak interdimeric exchange interactions mediated by hydrophobic chemical paths modulate the dimer EPR resonances giving rise to situations of strong, intermediate, and weak exchange.[24,25] Single crystal EPR spectroscopy of Cu(tda)(phen), analyzed on the basis of Anderson's exchange narrowing model[26,27] together with statistical arguments, showed that the transition from a weak exchange to a strong exchange situation provoked by the interdimer interaction J' depends also on the number of neighboring dimers in triplet states surrounding each dimeric unit.[25] However, the lack of a suitable diluted Cu(II) system isomorphous to pure Cu(tda)(phen) precluded us to determine the hyperfine interaction parameters associated with the copper nuclei and the ZFS. These inconveniences were overcome by proposing a simplified model that neglected the hyperfine interaction and assumed the ZFS as entirely determined by a dipole–dipole interaction under the point dipole approximation. Although these assumptions reproduced fairly well the experimental data, some discrepancies between the experimental and simulated EPR spectra still remain, likely due to the distinct approximations used in our model.

We report here the synthesis and X-ray characterization of the dimeric zinc(II) compound $[Zn(tda)(phen)]_2 \cdot H_2tda$, hereafter Zn(tda)(phen), isomorphous to Cu(tda)(phen), and single crystal EPR spectroscopy of Zn(tda)(phen) doped with Cu(II) ions, hereafter Cu : Zn(tda)(phen). The doping of Zn(tda)(phen) was performed at high Cu : Zn ratios (1 : 5) so as to enable the observation of EPR spectra associated with mononuclear and dinuclear Cu(II) species. This allowed us to completely determine the magnitudes associated with all the interactions contributing to the energy of the system as well as the subtle effects caused by covalency on the ZFS of the dinuclear units. The new data are used to propose a theoretical model that includes now the hyperfine interaction and covalency effects that explain the transition occurring when a copper pair is sensitive to interdimeric exchange interactions in an extended lattice.

Experimental section

Materials

All chemicals, of commercially available reagent grade, were used as received. Water was purified by a Millipore Milli-Q system.

Preparation of Zn(tda)(phen)

Single crystals of Zn(tda)(phen) were prepared as reported previously for the isomorphous Cu(tda)(phen) but using half the reported concentrations in order to slow down crystallization, which otherwise occurred within one to two hours.[24] This procedure yielded suitable single crystals for X-ray diffraction.

Preparation of Cu : Zn(tda)(phen)

Single crystals of Zn(tda)(phen) doped with copper(II) impurities were prepared by mixing solutions of Cu(tda)(phen) and Zn(tda)(phen), both prepared as described above for Zn(tda)(phen), in a Cu : Zn ratio of 1 : 5. This procedure yielded single crystals of ~0.2 × 0.2 × 0.5 mm, which were suitable for the single crystal EPR experiment.

Crystallography

Single crystal XRD data were collected using a Bruker Smart CCD area detector using Mo Kα radiation (λ = 0.71073 Å) (Diffractometer control: SMART; Data reduction: SAINT; Absorption correction: SADABS).[28]

The structure was solved by direct methods (SHELXS-97)[29] and refined by full-matrix least-squares on F^2 (SHELXL-2015).[30] Graphic material was produced using SHELXTL.[28] The acidic hydrogen bonded to oxygen in the thiodiacetic acid molecule was found using a Fourier-difference map and refined isotropically with the restrained O–H distance (0.85(1) Å); those attached to carbon were positioned theoretically and allowed to ride during refinement, with $U_{iso}(H) = 1.2 \times U_{eq}$(Host). The H_2tda molecule presents the C_2 symmetry, being bisected by a twofold axis through its central sulfur atom, thus rendering only one-half of the molecule independent.

A complete set of the results of the XRD crystallographic structural data has been deposited at the Cambridge Structural Database, CSD, in CIF format (deposition number CCDC 1055076). Details on the data collection procedures, structural determination methods, and structure refinement are given in the ESI, Table S1.†

The morphology of the single crystals, required to orient the sample for the single crystal EPR experiment, was determined by measuring the angles between the crystal faces using a Carl Zeiss Axiolab goniometric microscope. The monoclinic crystals are elongated prisms that grow along the c-axis and have lateral faces (110) and (1−10), with the angle between the ca^* plane ($a^* = b \times c$) and the (110) plane being 36.9°.

EPR measurements

X-band CW-EPR spectra of oriented single crystals of Cu : Zn-(tda)(phen) were recorded at room temperature on a Bruker EMX-Plus spectrometer equipped with a rectangular cavity with 100 kHz field modulation. Spectra were recorded in the a^*b ($a^* = b \times c$), ca^* and cb crystal planes by gluing the (110) face of a single crystal to a specially designed triangular-prismatic Rexolite sample holder (see Fig. S1†) with an angle of 36.9° (see above). The sample holder was glued to the tip of a 4 mm quartz EPR tube which was previously flattened by careful sanding, and the tube was introduced into the resonant cavity of the spectrometer attached to a goniometer which allowed rotating the crystal in 5° intervals in the three crystal planes.[31] EPR spectra were analyzed with the EasySpin toolbox and home-made programs based on MATLAB®.[32]

Electronic structure calculations

Density functional theory calculations were performed based on the structure of a single complete $[Cu(tda)(phen)]_2$ dimer.[24] Calculations were performed with the ORCA program[33] using the B3LYP (20% exact Hartree–Fock exchange, HFX),[34–36] TPSSh (10% exact HFX),[37,38] TPSS0 (25% exact HFX), ωB97x (range-separated functional with 15.77% HFX at a short range and 100% at a long-range)[39] and B2PLYP (a perturbatively corrected double-hybrid with 53% HFX)[40] functionals. The relativistic effects were included within the ZORA approximation[41,42] for which specially recontracted basis sets were used (SV_ZORA, TZV_ZORA or QZV_ZORA, as implemented in ORCA)[43] with polarization functions taken from the TZVP basis set.[44]

Results and discussion

Crystal and molecular structures

Crystals of Zn(tda)(phen) consist of dimeric units of [Zn(II)-(tda)(phen)]$_2$, connected by H_2tda molecules into chains parallel to [103]. The structure is isomorphous to its Cu(II) analogue,[24] sharing most of the general structural aspects, with the obvious metric differences in the cation environment. Fig. 1 shows the structure of the dinuclear unit and Table S2† gives some selected coordination bond lengths. The dinuclear unit displays a crystallographic center of symmetry linking the two constituent moieties with each zinc atom residing in a distorted N_2O_3S octahedral environment. The equatorial positions are occupied by the phen nitrogen atoms (N1 and N2), and by two oxygen atoms of the tda ligand (O2A and O4A) defining some kind of a flat tetrahedron (∠N1–Zn1–O2A: 173.4(2)°, ∠N2–Zn1–O4A: 164.2(2)°), with a maximum deviation from the mean plane of 0.09(1) Å for N2, and 0.16(1) Å for the Zn1 cation. The axial positions are occupied by the thioether sulfur atom (S1A) and a bridging carboxylate oxygen (O2A) of the neighboring ligand bonded to Zn1 [0.5 − x, 0.5 − y, −z], both atoms being fairly away from the normal plane (∠S1A–Zn1–O2A′: 155.5(2)°). The dimeric structure shows two Zn(II) centers bridged by two O-atoms of carboxylate groups in a bi-bridging mode, with C1A–O2A [1.284(2) Å] significantly longer than C1A–O1A [1.216(2) Å] as expected for this type of bonding. The dimer exhibits a (μ_2-oxo) Zn1–O_2–Zn1[0.5 − x, 0.5 − y, −z] ring which includes the center of symmetry at [0.25, 0.25, 0] with a Zn···Zn separation of 3.235(1) Å and a Zn–O–Zn bridging angle of 101.3(1)°. The two five-membered chelate rings with a common Zn–S bond in each tda are roughly planar, in a "butterfly" conformation with a dihedral angle between the least-squares planes of 93.3(1)°.

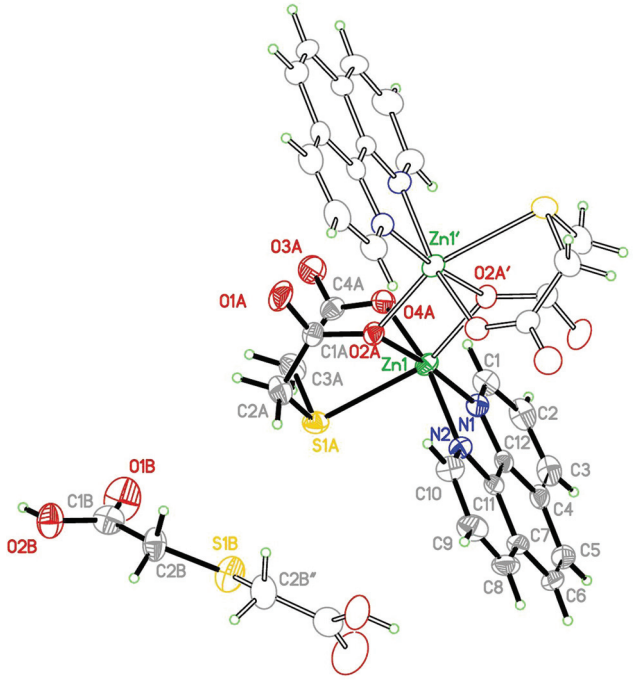

Fig. 1 Asymmetric units in Zn(tda)(phen). Displacement ellipsoids drawn at a 40%. Symmetry codes: ′: −x + 1/2, −y + 1/2, −z; ″: −x, y, −z + 1/2.

To understand the single crystal EPR experiment of the doped compound, it is important to note that Cu(tda)(phen) and Zn(tda)(phen) show four chemically identical dimers in the unit cell related to the symmetry operation of the space group $C2/c$ labeled as A, A′,B and B′. The copper dimers that are related to a translation (A–A′, or B–B′) are magnetically equivalent. In contrast, dimers A and B related to a 180° rotation around the b crystal axis plus a translation (0, 0, 1/2) are magnetically inequivalent. However, as described below, the phen planes of A- and B-type dimers, and therefore the equatorial ligand planes on each Zn and Cu atoms, are nearly parallel, making the **g**- and **A**-matrices of the copper dimers A and B indistinguishable within spectral resolution in the EPR experiment.

The phenanthroline planes between molecules of the same dimer type (A or B) are 3.389 Å apart in Zn(tda)(phen) (3.431 Å for Cu(tda)(phen)), whereas the phenanthroline planes of different dimer types (A–B) deviate by 3.70° (4.32° for Cu(tda)-(phen)), with the shortest distance between them being

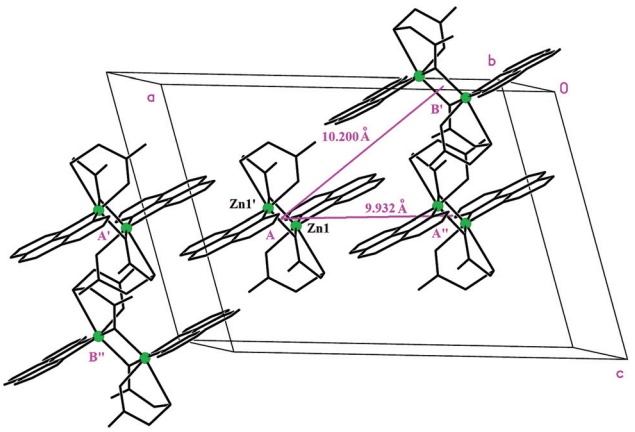

Fig. 2 Perspective of the crystal unit cell showing a Zn(tda)(phen) dimer with its four nearest neighbors interacting through hydrophobic interactions.

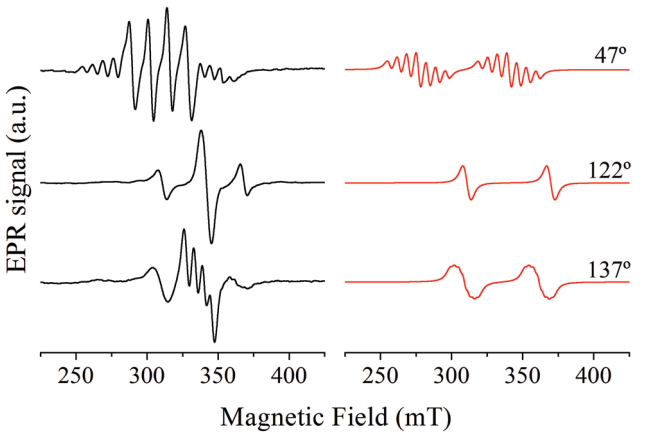

Fig. 3 Representative single crystal EPR spectra taken in the *ca** crystal plane where all the copper sites are magnetically equivalent (left panel) together with simulation of the satellite lines (right panel). The angles indicate the magnetic field orientation relative to the *c* crystal axis.

3.226 Å (3.482 Å for Cu(tda)(phen)). These distances strongly suggest delocalized π–π interactions between the aromatic planes. Thus, the dimer A(B) may interact with two type A(B) dimers and two type B(A) dimers (Fig. 2), with distances between dimers (measured from their inversion centers) being 9.932 and 10.200 Å for A–A(B–B) and A–B dimers, respectively (10.291 and 12.040 Å for Cu(tda)(phen)). Similarly to Cu(tda)(phen), nonadjacent A and B dimers in Zn(tda)(phen) are also bridged by a long mixed chemical path involving two hydrogen bonds (O–H···O distance = 2.58(6) Å, O–H···O angle = 177(6)°) and a thiodiacetic acid molecule (Fig. S2†), forming chains along the [103] direction, which interact with each other *via* a number of short contacts of the C–H···O type (see Table S3† for details). This chemical path of 15 diamagnetic atoms was discarded as the superexchange path in Cu(tda)(phen).[25]

An extremely similar $[Zn(phen)(tda)]_2$ dimeric unit has been reported by Grirrane *et al.* (Fig. S3†),[45] a structure where the dimers are linked by 5 disordered water molecules filling the interdimeric voids and providing multiple H-bonds to end up in a 3D H-bonded structure.

Single crystal EPR measurements

The representative single crystal EPR spectra of Cu : Zn(tda)(phen) recorded in the *ca** plane are shown in Fig. 3, left panel. The spectra show a central signal composed of one to four resonances with equal intensities, as expected for isolated mononuclear Cu(II) ions (S = 1/2, I = 3/2), flanked by less intense satellite signals. The latter are composed of one to seven resonances – although not all are observed due to overlapping with the central quartet – with a 1 : 2 : 3 : 4 : 3 : 2 : 1 intensity pattern, typical of a S = 1 electron spin coupled with two equivalent Cu(II) nuclei.[20] The central quartets and the satellite lines correspond to Cu–Zn heterodimers and to Cu–Cu homodimers, respectively.

The EPR spectra in the *cb* and *a*b* crystal planes (not shown), where the copper centers are magnetically inequivalent, showed only one central quartet for every magnetic field orientation as in the *ca** crystal plane, indicating that the EPR experiment cannot resolve the resonance lines corresponding to magnetically inequivalent copper ions. The reasons for this are explained in the Crystal and molecular structure section.

The central quartets corresponding to Cu–Zn heterodimers were analyzed assuming a Hamiltonian including Zeeman term and hyperfine interaction with the copper nucleus

$$H = \mu_B \mathbf{S}_1 \cdot \mathbf{g}_1 \cdot \mathbf{B} + \mathbf{S}_1 \cdot \mathbf{A}_1 \cdot \mathbf{I}_1 \quad (1)$$

where the subscript 1 stands for those Cu(II) ions that substitutionally occupy the position corresponding to Zn1 in Fig. 1, and the other symbols have their usual meaning in EPR. The fact that each dimeric unit may present a Cu(II) ion substituting the positions corresponding to Zn1′ (Fig. 1) is omitted in eqn (1), as Zn1 and Zn1′ are related to an inversion center and hence indistinguishable in the EPR experiment. Also, the sum of all the unit cells of the crystal lattice, as well as the sum of all the symmetry related dinuclear units have been omitted for simplicity.

The least-squares fitting of four equidistant Gaussian-shaped resonance lines to the central quartet spectra indicated that the experimental resonance positions are well simulated assuming eqn (1) up to the first order approximation, in which case the positions of the quartet resonance lines are given by $B_0 + aM_I$, (M_I = ±3/2, ±1/2), where B_0 and a are the gravity center and the hyperfine spacing of the quartet, respectively. The angular variations of the g^2-factor ($g = h\nu/\mu_B B_0$) and the g^2K^2-factor ($K = ag\mu_B/h$) obtained by this procedure are shown in Fig. 4 and S4,† respectively.

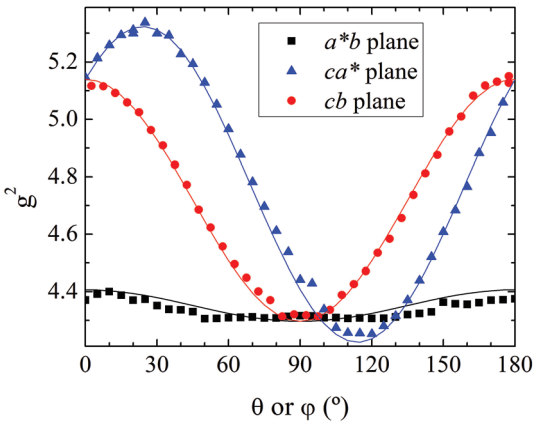

Fig. 4 Angular variation of the g^2-factor in the three crystal planes of Cu : Zn(tda)(phen).

The components of the $\mathbf{g}^2$-matrix were obtained by least-squares fitting a second-rank tensor to the data in Fig. 4

$$\begin{aligned} g^2(\theta,\varphi) = \mathbf{h}^{\mathrm{T}}\cdot\mathbf{g}\cdot\mathbf{g}^{\mathrm{T}}\cdot\mathbf{h} = {g_{xx}}^2 \sin^2\theta\cos^2\varphi \\ + {g_{yy}}^2 \sin^2\theta\sin^2\varphi + {g_{zz}}^2 \cos^2\theta \\ + 2{g_{xy}}^2 \sin^2\theta\cos\varphi\sin\varphi + 2{g_{zx}}^2\sin\theta\cos\varphi\cos\theta \\ + 2{g_{zy}}^2\sin\theta\sin\varphi\cos\theta \end{aligned} \quad (2)$$

in which $\mathbf{h} = \mathbf{B}/|\mathbf{B}|$ is the magnetic field orientation, and the superscript T stands for transpose. A similar procedure was employed to obtain the components of the **A**-matrix by the least-squares fitting equation $g^2K^2 = \mathbf{h}^{\mathrm{T}}\cdot\mathbf{g}\cdot\mathbf{A}^{\mathrm{T}}\cdot\mathbf{A}\cdot\mathbf{g}^{\mathrm{T}}\cdot\mathbf{h}$ to the data (Fig. S4†). Eigenvalues and eigenvectors for the **g**- and **A**-matrices were obtained by usual matrix algebra (Table 1), and are the same, within the experimental error, for the copper ions present in A- and B-type dimers. As explained above, this is due to the fact that the normal to the square ligand planes of the symmetry related metal centers in Cu(tda)(phen) and Zn(tda)(phen) are nearly coincident (the angle between normals ~5°). Both **g**- and **A**-matrices show roughly an axial symmetry with the $g_{||}$ and $A_{||}$ eigenvectors nearly coincident with the normal to the equatorial copper ligand planes, indicating a d($x^2 - y^2$) ground state, as expected for a Cu(II) ion in a nearly square planar coordination.

Table 1 Eigenvalues and eigenvectors (bold) of the molecular **g**- and **A**-matrices of the Cu(II) ion in the Cu–Zn heterodimer and the **D**-matrix of the Cu–Cu homodimer. The parameters are given in the experimental *a*bc* coordinate system. The D and E parameters correspond to $D = 3/2D_3$, and $E = 1/2(D_1 - D_2)$

$g_1 = 2.055(4)$	$\mathbf{g}_1 = [0.912, 0.02, -0.408]$
$g_2 = 2.073(4)$	$\mathbf{g}_2 = [0.01, -0.999, -0.00]$
$g_3 = 2.307(5)$	$\mathbf{g}_3 = [0.408, 0.012, 0.912]$
$A_1 = 19(10)$ MHz	$\mathbf{a}_1 = [-0.932, -0.009, 0.3625]$
$A_2 = 15(10)$ MHz	$\mathbf{a}_2 = [-0.008, 1.00, 0.005]$
$A_3 = 442(5)$ MHz	$\mathbf{a}_3 = [0.3625, -0.001, 0.932]$
$D_1 = 562(50)$ MHz	$\mathbf{d}_1 = [-0.8760, -0.2204, 0.4290]$
$D_2 = 753(60)$ MHz	$\mathbf{d}_2 = [-0.0629, -0.8297, -0.5546]$
$D_3 = -1315(60)$ MHz	$\mathbf{d}_3 = [0.4782, -0.5128, 0.7129]$
$D = -1973$ MHz (-0.0658 cm^{-1})	
$E = -96$ MHz (-0.0032 cm^{-1})	
$E/D = 0.048$	

The satellite signals corresponding to the Cu–Cu homodimer present in Cu : Zn(tda)(phen) were analyzed assuming the spin Hamiltonian

$$\boldsymbol{H} = \mu_{\mathrm{B}}\mathbf{S}\cdot\mathbf{g}\cdot\mathbf{B} + \mathbf{S}\cdot\mathbf{A}/2\cdot\mathbf{I}_1 + \mathbf{S}\cdot\mathbf{A}/2\cdot\mathbf{I}_{1'} + \mathbf{S}\cdot\mathbf{D}\cdot\mathbf{S} \quad (3)$$

where $\mathbf{g} = \mathbf{g}_1 = \mathbf{g}_{1'}$, $\mathbf{S} = \mathbf{S}_1 + \mathbf{S}_{1'}$, $\mathbf{A} = \mathbf{A}_1 = \mathbf{A}_{1'}$, and **D** is a matrix representing the dipole–dipole interaction. Anisotropic and antisymmetric exchange interactions are excluded in eqn (3) because of the small value of the intradimer exchange interaction ($J = +3.2$ cm^{-1})[24] and the inversion center between Cu1 and Cu1′, respectively.[20] The **g**- and **A**-matrices in eqn (3) were assumed to be those determined for the heterodimer species, as the homodimer spectra resolution precluded us to follow the experimental procedure used for the heterodimer species. When possible, the ZFS was evaluated from the separation δ between the gravity centers corresponding to the two groups of satellite resonance lines. For these cases where only one resonance group was clearly resolved, δ was calculated as $2(B_i - B_0)$ where B_i corresponded to either the low- or high-field resonance group and B_0 to the gravity center of the heterodimer signals. The experimental angular variation of **D** was analyzed by assuming eqn (3) up to first order, $\delta = 3\mathbf{h}^{\mathrm{T}}\cdot\mathbf{g}\cdot\mathbf{D}\cdot\mathbf{g}^{\mathrm{T}}\cdot\mathbf{h}/g^2$, following similar procedures to those explained for **g**- and **A**-matrices (Fig. S5,† Table 1). Simulations of the representative spectra shown in Fig. 3, left panel, using the parameters given in Table 1, are shown in the right panel of the same figure and show a good agreement with the experimental satellite lines. It is concluded that the doping procedure does not alter significantly the structure of the copper sites as EPR simulations were performed assuming identical **g**- and **A**-matrices for the copper sites in the hetero- and homodimers.

ZFS: point dipole approximation and distributed dipole model

As previously analyzed,[25] the ZFS of [Cu(tda)(phen)]$_2$ was assumed to be determined by dipole–dipole interaction under the point dipole approximation. Fig. 5 shows the angular variation of the **D**-matrix expected for [Cu(tda)(phen)]$_2$ under the point dipole approximation (blue line) together with that obtained from the experimental data (black line). As shown, the point dipole approximation predicts an order of magnitude of the ZFS along with a reasonable angular variation, but clearly other factors should be taken into consideration for a full interpretation of the experimental data. We considered that these discrepancies were due to spin delocalization onto the copper ligands; **g**- and **A**-matrices results indicate that the unpaired spin is in a d($x^2 - y^2$) type orbital, and therefore only delocalization onto copper equatorial ligands was considered. With this in mind, we simulated the angular variation of the

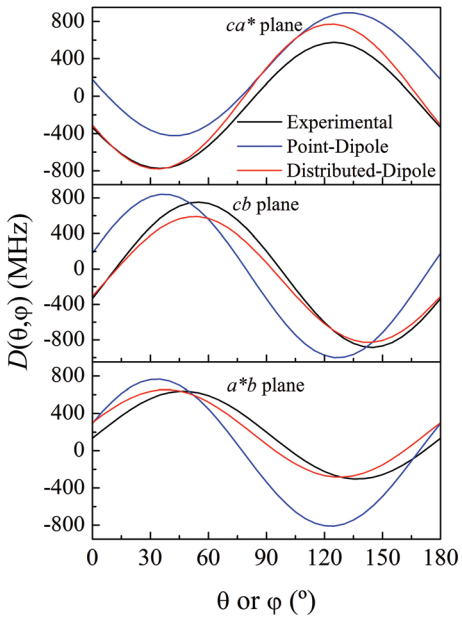

Fig. 5 Experimental angular variations (black lines) of **D** ($D(\theta,\varphi)$) in the *ca**, *cb* and *a*b* crystal planes, and simulations performed using the point-dipole approximation (blue) or a distributed dipole approximation (red) with best-fit spin populations shown in Table 2.

experimental **D**-matrix (Fig. 5, black line) assuming the so-called distributed dipole model[46–49]

$$\mathbf{D}_{ij} = \frac{\mu_0}{4\pi}\mu_B{}^2\left(\frac{\mathbf{g}_i^T\cdot\mathbf{g}_j - 3\left(\mathbf{g}_i\cdot\hat{\mathbf{r}}_{ij}\right)\left(\mathbf{g}_j\cdot\hat{\mathbf{r}}_{ij}\right)^T}{r_{ij}^3}\right) \qquad (4)$$

$$\mathbf{D} = \sum_{i,j}\rho_i\rho_j\mathbf{D}_{ij}$$

where ρ_i is the unpaired spin population on one of the Cu atoms of the dimer and its equatorial ligands, ρ_j is the same but for the other Cu atom, and $\mathbf{D}_{ij}$ is the dipole–dipole interaction matrix under the point dipole approximation between two unpaired electron spins of atoms *i* and *j*. The least squares fitting of eqn (4) to the data in Fig. 5 (red lines) yielded the spin populations ρ_i shown in Table 2. As shown in Fig. 5, the distributed dipole model gives a better description of the angular variation of **D** than that of the point dipole approximation, provided that the spin populations on the copper atom and its equatorial ligands are meaningful. Therefore, we performed electronic structure calculations to compare the spin populations predicted theoretically with those obtained from fitting eqn (4) to the data. The results obtained with different functionals and basis sets show that the spin populations obtained from the distributed dipole model are in good agreement with those calculated by DFT. The selected results obtained with the TPSSh and ωB97x functionals are shown in Table 2, while the complete set of calculated spin populations is shown in Table S4.† The calculated **g**- and **A**-matrices, as well as the *D* and *E*/*D* ZFS parameters, are shown in Table S5† together with the experimental values.

Table 2 Spin populations obtained from the distributed dipole model along with populations calculated by DFT. Calculations were performed using the $[Cu(tda)(phen)]_2$ structural data[24]

Atom	TPSSh ρ_S	ωB97x ρ_S	Fit to experimental **D**-matrix ρ_S
Cu	0.686	0.691	**0.657**
N1	0.069	0.070	**0.066**
N2	0.064	0.065	**0.066**
O2	0.068	0.067	**0.100**
O4	0.085	0.084	**0.110**

Calculations given in Table S5† show that all the functionals underestimate the *D* parameter, likely because the ORCA program calculates the dipolar matrix using the free electron g_e value,[47] instead of the anisotropic **g**-matrix associated with each spin (see eqn (4)). In our case we obtained a good agreement between the experiment and theory using anisotropic **g**-matrices, as proposed by other authors.[20,50] In any case, the spin populations calculated using the functionals listed in Tables 2 and S4† are in good agreement with the values obtained from fitting eqn (4) to the data shown in Fig. 5. Our results suggest that in cases where the experimental data allow such details, it is more accurate to calculate the dipolar interaction using the distributed dipole approximation with accurate spin populations predicted by DFT than to rely on the DFT calculated dipolar interaction. Other authors have also used the distributed dipole model, but for the analysis of powder EPR spectra, in which certain subtle effects may not be noticeable, or single crystal EPR spectra in highly symmetrical crystal environments, relying on analytical formulae possibly only due to the high symmetry.[46–49] Furthermore in the work of Smith *et al.* and Harris, only the ZFS parameter *D* was evaluated. In this work we show a complete analysis of the full angular variation of the dipolar interaction using the distributed dipole model, which allowed us to obtain the contribution to the **D**-matrix from spin populations on several atoms. Note that this information cannot be obtained only from the *D*-parameter.

Interdimeric exchange interaction

Fig. 6 shows representative single crystal EPR spectra obtained in the *ca** crystal plane of Cu : Zn(tda)(phen) (left) and $[Cu(tda)(phen)]_2$ (middle) for nearly the same magnetic field orientation. The changes in the EPR behavior that occur while moving from the magnetically diluted Cu : Zn(tda)(phen) (Fig. 6, left panel) to pure $[Cu(tda)(phen)]_2$ (Fig. 6, middle panel) are the results of the different spin concentrations of both systems. The spin states are well defined for Cu–Zn heterodimer ($S = 1/2$, central spectra in Fig. 6, left panel) and for Cu–Cu homodimer but with negligible interdimeric exchange interactions ($S = 1$, satellite lines in Fig. 6, left panel). The transition from $S = 1/2$ to $S = 1$ is caused solely by the intradimer exchange interaction ($J = +3.2$ cm^{-1}). The Cu–Cu homodimers with the non-negligible interdimeric

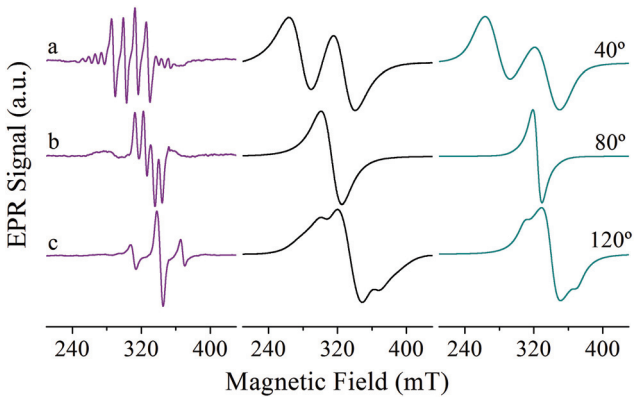

Fig. 6 Selected single crystal EPR spectra obtained in the *ca** crystal plane of Cu : Zn(tda)(phen) (left) and $[Cu(tda)(phen)]_2$ (middle) for nearly the same magnetic field orientations together with simulation of $[Cu(tda)(phen)]_2$ (right).

exchange interaction J' (Fig. 6, middle panel) can show two-line spectra for those situations with J' < ZFS (spectrum a), a single line for J' > ZFS (spectrum b) typical of an exchange-collapsed extended system,[31,51] or a mixture of the two previous situations (spectrum c).[25]

The changes experienced by the dimer EPR spectra when the dinuclear units are coupled by the interdimeric exchange interaction J' can be rationalized by computing the EPR spectrum within the linear response theory on the basis of the exchange narrowing model proposed by Anderson.[26,27] In this theory, the absorption spectrum in the frequency domain for an extended lattice of paramagnetic centers coupled by an unique exchange interaction is given by[52]

$$I(\omega,\omega_e) = \mathrm{Re}\{\mathbf{W}\cdot[i(\boldsymbol{\omega}-\omega\mathbf{E}+i\boldsymbol{\Gamma})+\boldsymbol{\pi}]^{-1}\cdot\mathbf{1}\} \quad (5)$$

where ω is the microwave frequency, ω_e is the exchange frequency ($\omega_e \approx J'/\hbar$), $\mathbf{W}$ is a vector whose components are the line intensities w_i, $\boldsymbol{\omega}$ and $\boldsymbol{\Gamma}$ are diagonal matrices whose elements are the absorption frequencies ω_i and linewidths Γ_i in the absence of exchange, respectively, $\mathbf{E}$ is the unit matrix, and $\boldsymbol{\pi}$ is a matrix whose elements give the transition probabilities between the resonance lines, and $\mathbf{1}$ is a vector with all components equal to one. It is important to note that except for the exchange frequencyω_e, which can only be coarsely estimated from the angular variation of the spectra, all the parameters involved in eqn (5) can be either evaluated (ω_i, Γ_i) or estimated (w_i) from the single crystal data of Cu : Zn(tda)(phen).

Eqn (5) has an analytical solution for the case of spectra showing two resonances which may arise from two interacting dissimilar S = 1/2 spins[53] or from interacting S = 1 dimers, both without an explicit hyperfine structure.[25] This simplest case can alternatively be obtained from generalized Bloch equations.[54] However, as the number of resonances increases, as is the case we are dealing with, an analytical solution first becomes impractical and soon impossible, and a numerical solution of eqn (5) is needed.

As said above, spectral simulation with eqn (5) accounts for the exchange narrowing phenomenon in the case of a dimer interacting with its neighbors through an unique exchange interaction.[23,53] However, in the case of $[Cu(tda)(phen)]_2$, eqn (5) fails to explain the angular variation of spectra such as the one shown in Fig. 6c, middle panel. This discrepancy between the experiment and simulation is due to the fact that the exchange interaction coupling of each dinuclear unit is not unique, which occurs when the S = 0 state is thermally accessible. Assuming no interdimeric exchange interactions, $[Cu(tda)(phen)]_2$ is a spin system in which the dimers can be either in singlet (S = 0) or in triplet (S = 1) states, with probabilities given by a Boltzmann distribution. As the singlet–triplet separation J in $[Cu(tda)(phen)]_2$ is 3.2 cm^{-1},[24] the Boltzmann distribution at room temperature gives approximately the same population for all the levels, and hence the probability of a dimer being in one of the triplet states is ρ = 0.75. Taking this into account, a central dimer in the triplet state (only in this state it will have an EPR signal), which is surrounded by four structural first neighbors connected by the superexchange paths (Fig. 2), will have a different number n of neighbors in the triplet state ($0 \le n \le 4$) with the probability p_n given by

$$p_n = \binom{4}{n}\rho^n(1-\rho)^{4-n} \quad (6)$$

This equation yields p_0 = 0.39%, p_1 = 4.69%, p_2 = 21.09%, p_3 = 42.19% and p_4 = 31.64% for ρ = 0.75. This means that most of the centers in a triplet state are surrounded by 3 dinuclear centers in a triplet state, but there are also triplet centers surrounded by 1, 2 and 4 dimers in the triplet state, and the exchange interaction between them is different, *i.e.*, $\omega_{e,n} = nJ'/\hbar$. In summary, eqn (5) describes the shape of the spectrum of an extended system in the presence of an unique exchange frequency ω_e, but if the system is composed of subsystems with different values of ω_e (*i.e.* $\omega_{e,n}$), given by populations of dimers with different number of triplet neighbors, then the spectrum becomes a sum of the spectra of each subsystem.

$$I(\omega) = \sum_n p_n I_n(\omega,\omega_{e,n}) \quad (7)$$

Simulations of the spectra of $[Cu(tda)(phen)]_2$ using eqn (7) are presented in Fig. 6, right panel. This simulation yielded J' = 0.010(1) cm^{-1}, slightly larger than the one reported in our previous work (J' = 0.0070(3)) cm^{-1},[25] with the difference being due to the previous use of the point dipole approximation. Our present data show that the point dipole approximation may fail not only in the estimation of distances[47] but also in the determination of exchange coupling constants by single crystal EPR spectroscopy using the exchange narrowing phenomenon. Exchange narrowing in EPR is the usual way to estimate very weak intercenter exchange interactions (<0.1 cm^{-1}) in undiluted magnetic systems. As shown in previous studies,[23,25,53,55] π–π interactions transmit weak exchange

interactions which modulate the magnetic properties of individual paramagnetic centers in extended lattices, and also, as evidenced for $[Cu(tda)(phen)]_2$, can transmit information about the spin-states of dimers, as the magnetic properties of a central dinuclear unit depend on the average number of neighbors in a triplet state. π–π interactions have been shown to play an important role in molecular spintronics, as reported for different magnetic molecules positioned on graphene or carbon nanotubes, and can also be used to design new magnetic materials with unprecedented physical properties.[6,56–59]

Conclusion

The single crystal EPR study of Cu : Zn(tda)(phen) has revealed the formation of Cu–Zn heterodimers and Cu–Cu homodimers in the diamagnetic zinc(II) host. The experiment allowed us to determine the anisotropic magnitudes **g**, **A**, and **D**. The information obtained from the diluted compound was used to evaluate the interdimeric exchange interaction J' between the dimeric units in $[Cu(tda)(phen)]_2$. This analysis yielded $J' = 0.010(1)$ cm^{-1}, slightly larger than that reported previously by us, $J' = 0.0070(3)$ cm^{-1}, which is ascribed undoubtedly to the use of the point dipole approximation in our previous calculations. Best simulation results were obtained using the distributed dipole model, which takes into account spin delocalization on the copper ligands due to covalency, showing clearly that the point dipole approximation can be used only to estimate an order of magnitude of exchange coupling constants by single crystal EPR spectroscopy. These results are relevant as they allow one to understand the influence of intercluster exchange interactions in the magnetic behavior of metal clusters synthesized as potential molecular magnets and in spintronics.

Acknowledgements

We thank FONCyT, CONICET, and CAI+D-UNL for financial support. N.I.N. and C.D.B. are members of CONICET-Argentina.

References

1 O. Kahn, *Molecular Magnetism*, VCH Publishers, New York, 1993.
2 A. Bencini and D. Gatteschi, *Electron Paramagnetic Resonance of Exchange Coupled Systems*, Springer-Verlag, Berlin, Germany, 1990.
3 D. Gatteschi, *Adv. Mater.*, 1994, **6**, 635–645.
4 J. Mroziński, *Coord. Chem. Rev.*, 2005, **249**, 2534–2548.
5 O. Kahn, *Angew. Chem., Int. Ed. Engl.*, 1985, **24**, 834–850.
6 M. Atzori, A. Serpe, P. Deplano, J. A. Schlueter and M. Laura Mercuri, *Inorg. Chem. Front.*, 2015, **2**, 108–115.
7 M. Castellano, R. Ruiz-García, J. Cano, J. Ferrando-Soria, E. Pardo, F. R. Fortea-Pérez, S. E. Stiriba, M. Julve and F. Lloret, *Acc. Chem. Res.*, 2015, **48**, 510–520.
8 F. Meyer, S. Demeshko, G. Leibeling, B. Kersting, E. Kaifer and H. Pritzkow, *Chem. – Eur. J.*, 2005, **11**, 1518–1526.
9 E. Moreno Pineda, N. F. Chilton, R. Marx, M. Dörfel, D. O. Sells, P. Neugebauer, S.-D. Jiang, D. Collison, J. van Slageren, E. J. L. McInnes and R. E. P. Winpenny, *Nat. Commun.*, 2014, **5**, 5243.
10 J. Camarero and E. Coronado, *J. Mater. Chem.*, 2009, **19**, 1678–1684.
11 D. Cangussu, E. Pardo, M.-C. Dul, R. Lescouëzec, P. Herson, Y. Journaux, E. F. Pedroso, C. L. M. Pereira, H. O. Stumpf, M. Carmen Muñoz, R. Ruiz-García, J. Cano, M. Julve and F. Lloret, *Inorg. Chim. Acta*, 2008, **361**, 3394–3402.
12 A. V. Astashkin, B. O. Elmore, W. Fan, J. G. Guillemette and C. Feng, *J. Am. Chem. Soc.*, 2010, **132**, 12059–12067.
13 A. K. Upadhyay, D. T. Petasis, D. M. Arciero, A. B. Hooper and M. P. Hendrich, *J. Am. Chem. Soc.*, 2003, **125**, 1738–1747.
14 C. D. Brondino, M. G. Rivas, M. J. Romão, J. J. G. Moura and I. Moura, *Acc. Chem. Res.*, 2006, **39**, 788–796.
15 J. H. Van Wonderen, V. S. Oganesyan, N. J. Watmough, D. J. Richardson, A. J. Thomson and M. R. Cheesman, *Biochem. J.*, 2013, **451**, 389–394.
16 M. C. Gómez, N. I. Neuman, S. D. Dalosto, P. J. González, J. G. Moura, A. C. Rizzi and C. D. Brondino, *J. Biol. Inorg. Chem.*, 2015, **20**, 233–242.
17 D. L. Reger, A. E. Pascui, M. D. Smith, J. Jezierska and A. Ozarowski, *Inorg. Chem.*, 2012, **51**, 7966–7968.
18 B. Bleaney and K. D. Bowers, *Proc. R. Soc. London, Ser. A*, 1952, **214**, 451–465.
19 C. Núñez, R. Bastida, A. Macías, L. Valencia, N. I. Neuman, A. C. Rizzi, C. D. Brondino, P. J. González, J. L. Capelo and C. Lodeiro, *Dalton Trans.*, 2010, **39**, 11654–11663.
20 T. D. Smith and J. R. Pilbrow, *Coord. Chem. Rev.*, 1974, **13**, 173–278.
21 R. Calvo, J. E. Abud, R. P. Sartoris and R. C. Santana, *Phys. Rev. B: Condens. Matter*, 2011, **84**, 104433–104445.
22 C. D. Brondino, R. Calvo and E. J. Baran, *Chem. Phys. Lett.*, 1997, **271**, 51–54.
23 N. I. Neuman, V. G. Franco, F. M. Ferroni, R. Baggio, M. C. G. Passeggi, A. C. Rizzi and C. D. Brondino, *J. Phys. Chem. A*, 2012, **116**, 12314–12320.
24 R. Baggio, M. T. Garland, J. Manzur, O. Peña, M. Perec, E. Spodine and A. Vega, *Inorg. Chim. Acta*, 1999, **286**, 74–79.
25 N. I. Neuman, M. Perec, P. J. González, M. C. G. Passeggi, A. C. Rizzi and C. D. Brondino, *J. Phys. Chem. A*, 2010, **114**, 13069–13075.
26 P. W. Anderson, *J. Phys. Soc. Jpn.*, 1954, **9**, 316–339.
27 P. W. Anderson and P. R. Weiss, *Rev. Mod. Phys.*, 1953, **25**, 269–276.
28 Bruker, *SMART-NT, SAINT-NT, SADABS, SHELXTL*, Bruker AXS Inc., Wisconsin, USA, 2001.
29 G. Sheldrick, *Acta Crystallogr., Sect. A: Fundam. Crystallogr.*, 2008, **64**, 112–122.

30 G. Sheldrick, *Acta Crystallogr., Sect. C: Cryst. Struct. Commun.*, 2015, **71**, 3–8.
31 J. M. Schveigkardt, A. C. Rizzi, O. E. Piro, E. E. Castellano, R. C. De Santana, R. Calvo and C. D. Brondino, *Eur. J. Inorg. Chem.*, 2002, 2913–2919.
32 S. Stoll and A. Schweiger, *J. Magn. Reson.*, 2006, **178**, 42–55.
33 F. Neese, *Wiley Interdiscip. Rev.: Comput. Mol. Sci.*, 2012, **2**, 73–78.
34 A. D. Becke, *J. Chem. Phys.*, 1993, **98**, 5648–5652.
35 C. Lee, W. Yang and R. G. Parr, *Phys. Rev. B: Condens. Matter*, 1988, **37**, 785–789.
36 B. Miehlich, A. Savin, H. Stoll and H. Preuss, *Chem. Phys. Lett.*, 1989, **157**, 200–206.
37 V. N. Staroverov, G. E. Scuseria, J. Tao and J. P. Perdew, *J. Chem. Phys.*, 2003, **119**, 12129–12137.
38 V. N. Staroverov, G. E. Scuseria, J. Tao and J. P. Perdew, *J. Chem. Phys.*, 2004, **121**, 11507–11507.
39 J.-D. Chai and M. Head-Gordon, *Phys. Chem. Chem. Phys.*, 2008, **10**, 6615–6620.
40 S. Grimme, *J. Chem. Phys.*, 2006, **124**, 034108.
41 E. v. Lenthe, E. J. Baerends and J. G. Snijders, *J. Chem. Phys.*, 1993, **99**, 4597–4610.
42 C. van Wüllen, *J. Chem. Phys.*, 1998, **109**, 392–399.
43 D. A. Pantazis, X.-Y. Chen, C. R. Landis and F. Neese, *J. Chem. Theory Comput.*, 2008, **4**, 908–919.
44 A. Schäfer, H. Horn and R. Ahlrichs, *J. Chem. Phys.*, 1992, **97**, 2571–2577.
45 A. Grirrane, A. Pastor, E. Álvarez, C. Mealli, A. Ienco and A. Galindo, *Inorg. Chem. Commun.*, 2006, **9**, 160–163.
46 P. Bertrand, P. Camensuli, C. More and B. Guigliarelli, *J. Am. Chem. Soc.*, 1996, **118**, 1426–1434.
47 C. Riplinger, J. P. Y. Kao, G. M. Rosen, V. Kathirvelu, G. R. Eaton, S. S. Eaton, A. Kutateladze and F. Neese, *J. Am. Chem. Soc.*, 2009, **131**, 10092–10106.
48 S. R. P. Smith and J. Owen, *J. Phys. C: Solid State Phys.*, 1971, **4**, 1399.
49 E. A. Harris, *J. Phys. C: Solid State Phys.*, 1972, **5**, 338.
50 A. Abragam and B. Bleaney, *Electron paramagnetic resonance of transition ions*, Dover Publications, New York, 1986.
51 A. C. Rizzi, O. E. Piro, E. E. Castellano, O. R. Nascimento and C. D. Brondino, *Inorg. Chim. Acta*, 2000, **305**, 19–25.
52 R. A. Sack, *Mol. Phys.*, 1958, **1**, 163–167.
53 C. D. Brondino, R. Calvo, A. M. Atria, E. Spodine, O. R. Nascimento and O. Peña, *Inorg. Chem.*, 1997, **36**, 3183–3189.
54 S. K. Hoffmann, A. Waśkowska and W. Hilczer, *Solid State Commun.*, 1990, **74**, 1359–1361.
55 C. D. Brondino, R. Calvo, A. M. Atria, E. Spodine and O. Peña, *Inorg. Chim. Acta*, 1995, **228**, 261–266.
56 S. M. Avdoshenko, I. N. Ioffe, G. Cuniberti, L. Dunsch and A. A. Popov, *ACS Nano*, 2011, **5**, 9939–9949.
57 M. Urdampilleta, S. Klayatskaya, M. Ruben and W. Wernsdorfer, *ACS Nano*, 2015, **9**, 4458–4464.
58 M. Urdampilleta, N.-V. Nguyen, J.-P. Cleuziou, S. Klyatskaya, M. Ruben and W. Wernsdorfer, *Int. J. Mol. Sci.*, 2011, **12**, 6656.
59 W. Wernsdorfer, N. Aliaga-Alcalde, D. N. Hendrickson and G. Christou, *Nature*, 2002, **416**, 406–409.